Molecular Biology of the Cell
Vol. 9, 2491–2507, September 1998

Organization of Highly Acetylated Chromatin around Sites of Heterogeneous Nuclear RNA Accumulation

Michael J. Hendzel, Michael J. Kruhlak, and David P. Bazett-Jones*

Departments of Anatomy and Medical Biochemistry, Faculty of Medicine, University of Calgary, Calgary, Alberta, Canada T2N 4N1

Submitted November 26, 1997; Accepted July 2, 1998
Monitoring Editor: Joseph Gall

Histones found within transcriptionally competent and active regions of the genome are highly acetylated. Moreover, these highly acetylated histones have very short half-lives. Thus, both histone acetyltransferases and histone deacetylases must enrich within or near these euchromatic regions of the interphase chromatids. Using an antibody specific for highly acetylated histone H3, we have investigated the organization of transcriptionally active and competent chromatin as well as nuclear histone acetyltransferase and deacetylase activities. We observe an exclusion of highly acetylated chromatin around the periphery of the nucleus and an enrichment near interchromatin granule clusters (IGCs). The highly acetylated chromatin is found in foci that may reflect the organization of highly acetylated chromatin into "chromonema" fibers. Transmission electron microscopy of Indian muntjac fibroblast cell nuclei indicates that the chromatin associated with the periphery of IGCs remains relatively condensed, most commonly found in domains containing chromatin folded beyond 30 nm. Using electron spectroscopic imaging, we demonstrate that IGCs are clusters of ribonucleoprotein particles. The individual granules comprise RNA-rich fibrils or globular regions that fold into individual granules. Quantitative analysis of individual granules indicates that they contain variable amounts of RNA estimated between 1.5 and >10 kb. We propose that interchromatin granules are heterogeneous nuclear RNA-containing particles, some of which may be pre-mRNA generated by nearby transcribed chromatin. An intermediary zone between the IGC and surrounding chromatin is described that contains factors with the potential to provide specificity to the localization of sequences near IGCs.

INTRODUCTION

The development of antibody and nucleic acid probes together with improved microscopic methodologies is rapidly advancing our understanding of the relationship between biochemical processes and complex nuclear compartments (see Clemson and Lawrence, 1996; Huang and Spector, 1996; Puvion and Puvion-Dutilleul, 1996; Spector, 1996; Strouboulis and Wolffe, 1996; Lamond and Earnshaw, 1998). In this respect, it is of particular interest to understand the general organization of euchromatin in interphase nuclei. An antibody specific for the highly acetylated species found within transcriptionally active and competent euchromatic regions of interphase chromatin has been developed (Boggs *et al.*, 1996). This antibody provides a tool to investigate the general organization of euchromatin.

There are several reasons to believe that highly acetylated chromatin may be spatially organized within the cell nucleus. There is emerging evidence that active genes are nonrandomly distributed within interphase chromosome territories (reviewed in Lamond and Earnshaw, 1998). A nonrandom organization of active genes should be reflected in the localization of highly acetylated chromatin within the cell nucleus. Biochemical experiments indicate that highly acetylated chromatin is organized differently than bulk chromatin. Nuclear fractionation experiments demonstrate that highly acetylated chromatin fragments are

* Corresponding author.

enriched in nuclear matrices (Hendzel *et al*., 1991) and that approximately half of the total bulk nuclear histone acetyltransferase and histone deacetylase activities are associated with the nuclear matrix (reviewed in Davie and Hendzel, 1994; Davie, 1996). Moreover, dynamic histone acetylation can proceed in vitro within endogenous nuclear matrix-associated chromatin when nuclear matrices are prepared by low-ionic-strength lysis of micrococcal nuclease-digested nuclei (Hendzel *et al*., 1994). These results implicate both chromatin and nonchromatin structures in the organization of transcription-associated histone acetylation.

There is increasing evidence that gene activity is nonrandomly organized within the cell nucleus (Clemson and Lawrence, 1996; Spector, 1996; Lamond and Earnshaw, 1998). Of particular interest, a spatial and functional relationship between intranuclear structures, termed interchromatin granule clusters (IGCs), and specific transcribed loci has been reported (Huang and Spector, 1991; Xing *et al*., 1993, 1995). IGCs, originally characterized by transmission electron microscopy (TEM) (Monneron and Bernhard, 1969, and references therein; Wassef, 1979), were more recently identified by indirect immunofluorescence and immunogold TEM as sites of splicing factor accumulation (Fakan *et al*., 1984; Spector, 1990; Spector *et al*., 1991). Subsequently, nuclear poly(A) RNA and specific endogenous pre-mRNAs were observed to accumulate within IGCs (Carter *et al*., 1991, 1993; Huang and Spector, 1991; Visa *et al*., 1993; Xing *et al*., 1993, 1995; Huang *et al*., 1994; Clemson and Lawrence, 1996). IGCs have been directly implicated in the trafficking of viral RNAs (reviewed in Bridge and Pettersson, 1996; Puvion and Puvion-Dutilleul, 1996; Ishov *et al*., 1997). Spliced pre-mRNAs from adenovirus late genes are observed to accumulate within enlarged IGCs (Bridge *et al*., 1996). Kinetic labeling data indicate that these spliced and polyadenylated RNAs accumulate within IGCs before transport to the cytoplasm (Bridge *et al*., 1996; Puvion and Puvion-Dutilleul, 1996; Nevins and Darnell, 1978). Most recently, the dynamic properties of IGCs have been described (Misteli *et al*., 1997). These studies directly demonstrate that IGCs supply splicing factors to surrounding gene loci. The collective implications of these studies are that transcription occurs largely, although perhaps not exclusively, on the immediate periphery of IGCs, and that IGCs are directly involved, at a number of levels, in mRNA biogenesis.

Although transcription can occur on the periphery of IGCs, and IGCs function as reservoirs that supply splicing factors to the surrounding chromatin, whether pre-mRNA also traffics through IGCs remains controversial for several reasons. First, although pulse labeling of nuclear RNA with [^{3}H]uridine demonstrates the presence of newly synthesized RNA on the periphery of IGCs (reviewed in Fakan and Puvion, 1980; Spector, 1990), accumulation within IGCs is generally not observed (Fakan and Bernhard, 1973; Fakan, 1994; Spector, 1990; although see Raska, 1995). Second, although poly(A) RNA is enriched in IGCs (Carter *et al*., 1993; Visa *et al*., 1993), at least some poly(A) RNA remains in IGCs for several hours after transcriptional inhibition (Huang *et al*., 1994; Fay *et al*., 1997). Poly(A) pre-mRNAs are generally characterized as short lived. Third, the vectorial transport of splicing factors from IGCs to transcriptionally active loci has been observed in living cells (Misteli *et al*., 1997). These and other data indicate that splicing occurs cotranscriptionally at sites of transcription (reviewed in Misteli and Spector, 1997), and that pre-mRNAs may not enter IGCs. Although the nature of the RNA within IGCs is controversial, it is clear that IGCs are functionally involved in the generation of mRNA. If IGCs are involved in the production of mRNA generally, then the organization of euchromatin should reflect a general association with the IGC compartment.

In this study, we have addressed several fundamental questions about the organization of euchromatin and its relationship with the IGC. First, using antibodies recognizing transcription-associated acetylated histone isoforms, we demonstrate an enrichment of highly acetylated chromatin and associated histone acetyltransferase and deacetylase activities on the periphery of the IGC. Highly acetylated chromatin is also notably excluded from the nuclear periphery and perinucleolar regions. Second, we demonstrate that these intranuclear regions, defined by heterochromatic boundaries, are enriched in transcriptional activity. Third, we demonstrate that interchromatin granules are RNA-containing particles comprising folded ribonucleoprotein (RNP) fibrils or globular subregions. Fourth, from quantitative analysis of nucleic acid content within individual granules of IGCs, we demonstrate that interchromatin granules are heterogeneous nuclear RNA (hnRNA)-containing particles. Our results are consistent with the involvement of IGCs in RNA production from a multitude of genes.

MATERIALS AND METHODS

Preparation of Cells for TEM

Cells were grown on a polypropylene surface (the cap of a 50-ml conical tube) to facilitate separation of the embedding medium from the growth surface under culture conditions recommended by American Type Culture Collection (ATCC; Rockville, MD). Cells were fixed with 1.0% paraformaldehyde in PBS (pH 7.5) for 30 min at room temperature. Cells were then dehydrated using a graded ethanol series. Whole cells were embedded in Quetol 651-NSA (Electron Microscopy Sciences, Ft. Washington, PA) by first dehydrating 4 h to overnight in Quetol 651 and then infiltrating overnight with the Quetol 651-NSA mix. Polymerization was performed at 60°C for 2 d. Sections were then cut using a diamond knife (Drukker [Edgecraft], Avondale, PA). Sections used for data collection were consistently near 30 nm in thickness. The consistency of section thickness was defined by two experimental barriers. An

upper limit of ~35 nm was imposed by high background generated by the mass of the embedding medium. A low limit of ~25 nm was imposed by the physical stability of the section. Images were recorded with a Zeiss (Thornwood, NY) EM902 electron microscope equipped with a prism–mirror–prism electron imaging spectrometer. It was operated at an accelerating voltage of 80 kV. A 600-μm condenser aperture, a 90-μm objective aperture, and a 15- to 20-eV energy-selecting slit aperture were used. Images were recorded at 13,000, 20,000, or 30,000× on SO-163 electron image film (Kodak, Rochester, NY) and developed in full-strength D-19 developer (Kodak) for 15 min at room temperature. In some instances, images were recorded digitally using a Gatan (Pleasanton, CA) 14-bit slow-scan charge-coupled device (CCD).

Indirect Immunofluorescence

Cells were cultured directly on glass coverslips under conditions recommended by ATCC. Cells were seeded onto coverslips, cultured overnight, and then fixed with 1.0% paraformaldehyde in PBS (pH 7.5) at room temperature for 5 min. Subsequently, cells were permeabilized in PBS containing 0.1% Triton X-100 for 5 min. Coverslips were inverted onto parafilm containing 25-μl drops of primary antibodies diluted in PBS or anti-SC-35 containing cell culture supernatant for 60 min at 22°C, washed three times in PBS, and then incubated a further 60 min in the presence of Cy3-anti-rabbit immunoglobulin G (IgG) and FITC-anti-mouse IgG, IgA, and IgM. Coverslips were washed again in PBS and then mounted onto slides using a 90% glycerol-PBS (pH 7.5)–based medium containing 1 mg/ml paraphenylenediamine and 1 μg/ml DAPI.

The antibody specific to highly acetylated forms of histone H3 has previously been characterized by Boggs *et al.* (1996) and shows a strong preference for the most highly acetylated species of histone H3 in mammalian tissue culture cell lines. A hybridoma expressing anti-SC-35 was obtained from ATCC. Tissue culture supernatants were used undiluted. The $TAF_{II}250$ antibody (Santa Cruz Biotechnology, Santa Cruz, CA) recognized a single band of ~250 KDa, as expected, and has been characterized previously (Mizzen *et al.*, 1996). The histone deacetylase 1 (HDAC1) antibody was obtained from Upstate Biotechnology (Lake Placid, NY). Results were verified using a second antibody provided by Dr. J. Davie (University of Manitoba, Winnipeg, Manitoba, Canada).

Digital Image Collection and Processing

TEM negatives were digitized, and net nitrogen and phosphorus maps were generated from energy loss images as described previously (Hendzel and Bazett-Jones, 1996). Quantitation was performed as described previously (Hendzel and Bazett-Jones, 1996), except that ribosomes were used as internal mass and phosphorus standards (see Abholhassani-Dadras *et al.*, 1996). Digital optical sectioning of nuclei was performed as described by Rattner *et al.* (1996) with the exception that the z-axis optical offsets between fluorescence channels was calculated and compensation was made at the data collection stage. Deconvolved images were obtained using Vaytek (Fairfield, IA) Digital Confocal Microscope version 2.5 for DOS software. Deconvolved images were rescaled to cover the entire 255-value gray range. Although the background generated on the CCD detector in unstained regions was subtracted from the image before rescaling, care was taken not to remove low-level signals within the cell nucleus present in the deconvolved images. In multicolor images that include a blue channel image (DAPI), it was necessary to enhance contrast. This leads to some compression of the dynamic range among the intensely and intermediately labeled sites. Although some quantitative information is preserved, it is best to view these images primarily as spatial maps reflecting the presence or absence of signal.

Quantitative Analysis of Phosphorus in Interchromatin Granules

The application of electron spectroscopic imaging (ESI) to the estimation of phosphorus and mass content in biological specimens using internal mass and phosphorus standards has been described previously (Bazett-Jones, 1992). Ribosomes, which contain 6600 atoms of phosphorus contributed by the ribosomal RNAs (Alberts *et al.*, 1994), were used as internal quantitative standards. Because the phosphorus contribution by protein phosphorylation is negligible relative to the phosphorus component of nucleic acid, a value of 6600 phosphorus atoms was used. Net values of phosphorus for interchromatin granules and ribosomes were obtained by measuring the integrated density of the particles in both 155-eV (phosphorus-enhanced) and 120-eV (mass-dependent) energy loss images. Mass dense particles found within IGCs were quantitated. To correct for slight exposure differences, the two images were normalized using the background signal produced by the embedding medium (which contains no phosphorus). Several ribosomes in close proximity to an IGC were used to obtain an average phosphorus integrated density. This was related to the integrated density of individual granules and used to calculate individual interchromatin granule particle mass and phosphorus contents. Granules that appeared elongated and may represent two partially overlapping granules were not included in the quantitation. Because the section thickness is only slightly larger than the mean granule diameter, most granules within a cluster were observed as individual granules, well resolved from neighboring particles.

RESULTS

Large-Scale Organization of the Fibroblast Cell Nucleus

Besides chromatin and the nucleoli, the predominant structure of the nucleoplasm is the IGC. These structures are recognized by a monoclonal antibody generated against SC-35 (Fu *et al.*, 1990; Spector *et al.*, 1991). We determined the overall organization of DNA within an Indian muntjac fibroblast cell nucleus and its relationship to the major nonchromatin structure, the IGC, by colabeling cells with anti-DNA and anti-SC35 antibodies. Figure 1 shows six individual digital optical sections passing through an MRC-5 fibroblast cell nucleus. The first two sections and the last section represent the upper and lower surfaces of the nucleus. The DNA staining (green) is enriched around the periphery of the cell nucleus where the majority of the condensed blocks of chromatin are observed (small arrows). DNA is absent from SC-35–containing domains (red) and is often depleted on their immediate periphery (large arrows). Apart from being present in larger nuclear speckles (IGCs), SC-35 is also found in numerous small foci, which are common in the planes above and below the larger nuclear speckles. The SC-35 domains (IGCs) are largely contained within sections 3 and 4, near and just below the midline of the cell nucleus. Similar observations on the organization of SC-35 domains have been reported previously in other fibroblast cell lines (Carter *et al.*, 1993).

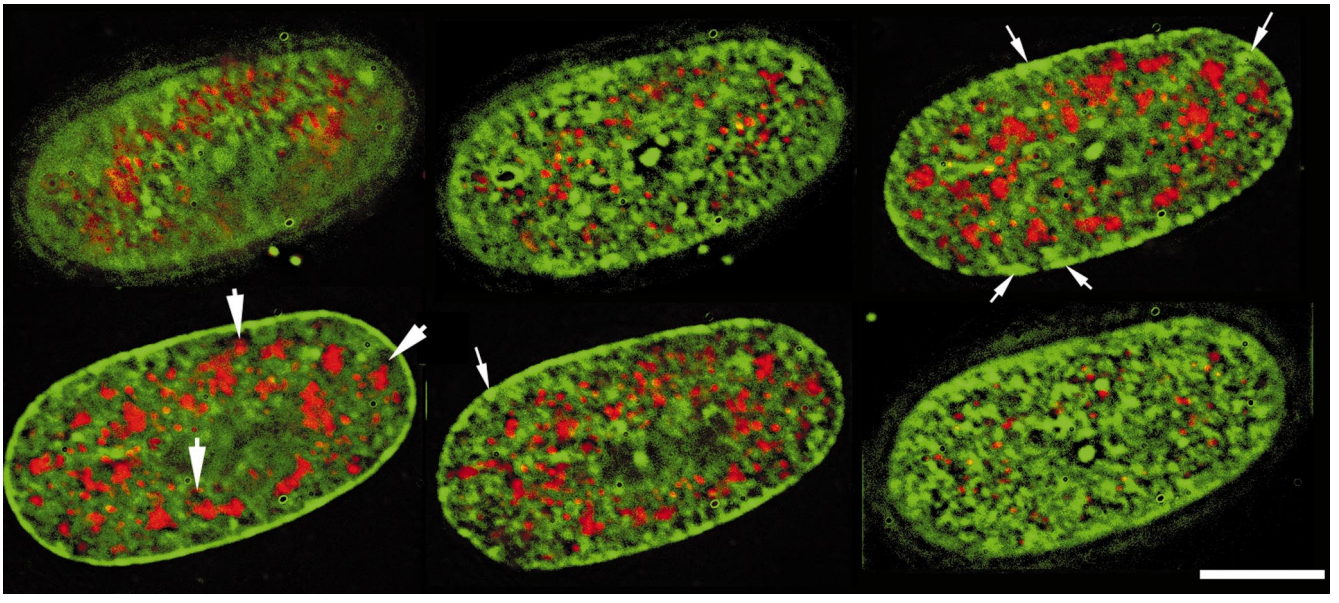

Figure 1. Organization of DNA within the fibroblast nucleus. Digitally deconvolved optical sections of 0.4 μm were independently collected for anti-DNA and anti-SC35 staining. The distribution of DNA is shown in green, and the distribution of SC-35 is shown in red. Sections are shown at 0.8-μm intervals and proceed from left to right. The first two images show sections farthest from the growth surface, and the last image represents the nuclear surface closest to the growth attachment site. The large arrows indicate chromatin-depleted regions, whereas the small arrows indicate regions of highly condensed chromatin. Bar, 10 μm.

Organization of Euchromatin

Elevated levels of histone acetylation are associated with euchromatic regions of mammalian chromosomes (reviewed in Jeppesen, 1997). For example, DNA probes isolated from mononucleosomes enriched in highly acetylated histones produce an R-banding pattern in metaphase chromosome spreads (Breneman *et al*., 1996). Similar observations have been made directly with acetylation-specific antibodies when chromosomes are maintained in a hyperacetylated state during mitosis (reviewed in Jeppesen, 1997). We used an antibody specific for acetylated lysines 9 and 14 of histone H3. This antibody recognizes principally the highest acetylated species of histone H3 (tri, tetra, and penta) on immunoblots (Boggs *et al*., 1996). When cells are labeled for immunofluorescence using this antibody, the epitope is dramatically increased by incubations with HDAC inhibitors. Furthermore, the epitope is nearly completely lost during prophase but can be maintained in mitotic chromosomes if cells are allowed to progress to M-phase in the presence of HDAC inhibitors (Kruhlak, Hendzel, and Bazett-Jones, unpublished observations). The epitope reappears in the chromatin post-mitotically just before the reassociation of RNA polymerase II and the resumption of transcription (Kruhlak *et al*., unpublished observations). These properties indicate that the in situ epitope also corresponds primarily to the highly acetylated histones associated with transcriptionally competent and transcriptionally active euchromatin. The antibody, therefore, makes a suitable probe to investigate the general organization of the functional euchromatin within the cell nucleus.

Indirect immunofluorescence using this antibody shows that highly acetylated chromatin is enriched in numerous foci and elongated foci scattered throughout the interphase nucleus (Figure 2; also see Figure 3B). This is somewhat surprising given that the levels of histone acetylation detected by this antibody are likely to drive the dissociation of fiber–fiber and intrafiber nucleosomal interactions in vitro (Garcia-Ramirez *et al*., 1995; Schwarz *et al*., 1996). Thus, we expected to see a more disperse distribution of the highly acetylated chromatin rather than structures, such as foci, which have relatively well-defined boundaries. However, there is accumulating evidence that even euchromatic regions of mammalian chromatin are compacted into complex higher-order fibers in situ (Belmont and Bruce, 1994; Robinett *et al*., 1996). The dimensions of the acetylated chromatin foci may reflect regions of high acetylation within such a higher-order structure.

The relative organization of DNA and SC-35 indicates that bulk chromatin is depleted at the periphery of IGCs. In contrast, several active gene probes specifically localize to these same regions (Huang and Spector, 1991; Xing *et al*., 1993, 1995). Thus, it was of interest to map the organization of highly acetylated chromatin relative to condensed chromatin, which can

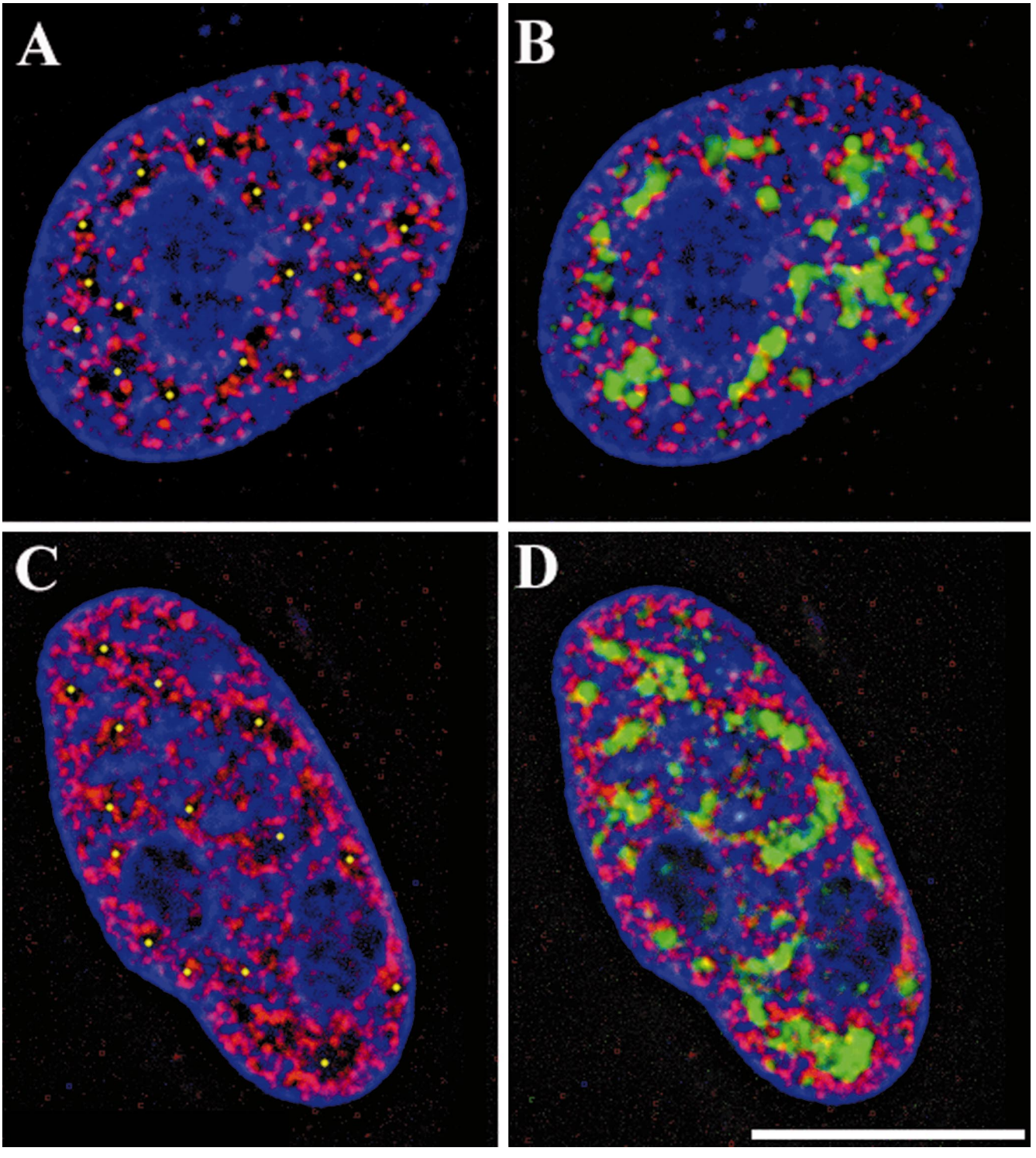

Figure 2. Organization of dynamically acetylated euchromatin in the fibroblast nucleus. Digital optical sections of 0.4 μm were collected from Indian muntjac fibroblast cell nuclei that were cultured in the absence (A and B) or presence (C and D) of 10 mM sodium butyrate for 60 min. Cells were stained with an antibody specific to highly acetylated histone H3 (red), anti-SC-35 (green), and DAPI (red). The yellow dots in A and C indicate the positions of chromatin-depleted regions of the cell nucleus that correspond to regions positive for SC-35 (C and D). Bar, 10 μm.

be visualized with DAPI, and IGCs, which can be visualized with the anti-SC-35 antibody. We find that highly acetylated chromatin is excluded from the immediate periphery of the nucleus (Figure 2). This region of the nucleus is particularly rich in heterochromatin and may be the major site of nuclear attachment for all of the interphase chromosomes (Ferreira *et al*., 1997). The non-nucleolar DAPI-depleted zones are primarily occupied by SC-35 (Figure 2A, yellow dots). Many of the acetylated histone foci localize on the border between the heterochromatic region and the SC-35 domain (Figure 2, A and B). Note, however, that the acetylated chromatin foci show minimal encroachment on the interior of the SC-35 domains, consistent with numerous other reports indicating an absence of DNA within IGCs (Thiry, 1993, and references therein).

Although transcriptionally active, competent chromatin is significantly enriched in highly acetylated histones when compared with bulk chromatin, this difference is dramatic when acetylation metabolism is analyzed. Specifically, transcriptionally active, and to a lesser extent transcriptionally competent, chromatin contain acetylated histone species that are characteristically dynamic (Boffa *et al*., 1990; Hendzel *et al*., 1991; reviewed in Davie and Hendzel, 1994). Consequently, incubations with HDAC inhibitors results in the rapid accumulation of highly acetylated histone species within this smaller fraction of the genome, followed by a slower accumulation of lower acetylated species throughout the remainder of the genome (Covault and Chalkley, 1980). We took advantage of the rapid accumulation of highly acetylated histones in transcriptionally active, competent chromatin to map the sites of the dynamic class of acetylated histone species. Frequently, brief incubations with HDAC inhibitors produced an enrichment in antibody labeling on the periphery of SC-35 domains that was striking enough to be visible directly in immunofluorescent images as rings of hyperacetylation. In digital optical sections, there is an obvious enrichment of hyperacetylated chromatin on the periphery of IGCs (Figure 2, C and D). If dynamic histone acetylation occurred principally in regions distant from IGCs, the labeling of the chromatin surrounding the IGC would be suppressed relative to nuclear sites hyperacetylated by treatment with HDAC inhibitors. Thus, we conclude that the class of chromatin that contains elevated steady-state levels of histone acetylation and is dynamically acetylated enriches on the periphery of IGCs.

Localization of Specific Nuclear Histone Acetyltransferases

The preceding data argue that the fibroblast cell nucleus has a specific organization. The heterochromatin forms structural contacts lining the surface of the nuclear lamina and the nucleolus. Intranuclear islands of heterochromatin further define boundaries of nuclear regions occupied by IGCs. The dynamically acetylated euchromatin preferentially occupies the nuclear regions proximal to the IGCs. Thus, we propose a working definition of an IGC-based compartment whose boundaries are defined by heterochromatic regions of the cell nucleus. We analyzed the subnuclear distribution of the $TAF_{II}250$ protein using heterochromatin and acetylated chromatin to define the boundaries of these putative compartments (Figure 3). The $TAF_{II}250$ protein associates with the TATA-binding protein and is, therefore, a component of RNA polymerase II promoter-associated complexes (Ruppert *et al*., 1993). Moreover, the $TAF_{II}250$ protein is the major histone acetyltransferase activity of mammalian cell extracts when in vitro gel activity assays are used (Mizzen *et al*., 1996). If the HAT activity of $TAF_{II}250$ is responsible for significant amounts of histone acetylation in situ, the dramatic increase in acetylation on the periphery of IGCs, observed during brief treatments with HDAC inhibitors, suggests that $TAF_{II}250$ should enrich near IGCs. Figure 3A–C shows the distributions, in a 0.4-μm-thick digital optical section, of DAPI-stained chromatin (Figure 3A), acetylated H3 containing chromatin (Figure 3B), and $TAF_{II}250$ (Figure 3C). Although the acetylated chromatin and $TAF_{II}250$ protein have a superficially similar organization, the composite image (Figure 3D) and Figure 3F–I demonstrate that a significant amount of the $TAF_{II}250$ protein (green) localizes to regions distinct from both the highly acetylated chromatin (red) and the condensed heterochromatin (blue). This result is emphasized at higher

Figure 3 (facing page). Relative organization of the $TAF_{II}250$ histone acetyltranferase and substrate chromatin in the fibroblast cell nucleus. A digital optical section of an Indian muntjac fibroblast cell nucleus costained with anti-$TAF_{II}250$, antiacetylated histone H3, and DAPI is shown. (A–C) Distributions of DAPI (A), highly acetylated histone H3 (B), and $TAF_{II}250$ (C), independently. (D) Composite image with DAPI (blue), highly acetylated H3 (red), and $TAF_{II}250$ (green). (E) Spatial relationship between DAPI-stained bulk chromatin (white) and highly acetylated chromatin. Images were subjected to thresholding, and the extent of overlap and independence was determined for the highly acetylated H3 distribution. Regions that are blue indicate regions where DAPI signal was detected. Regions that are red indicate regions where no DAPI signal was detected after digital deconvolution. (F) Spatial relationship between the $TAF_{II}250$ and chromatin distributions. The DAPI distribution is shown in white. Regions that contain $TAF_{II}250$ but neither DAPI nor acetylated histone H3 are shown as green. Regions that contain both $TAF_{II}250$ and highly acetylated histone H3 are shown as red, whereas regions that contain both $TAF_{II}250$ and DAPI but no detectable acetylated histone H3 are shown as blue. (G–I) Subregion at 4× magnification. Composites are shown in which DAPI is blue, highly acetylated histone H3 is red, and $TAF_{II}250$ is green. The yellow dots in A and G indicate the positions of chromatin-depleted extranucleolar regions that are likely to contain IGCs. The red dots in A indicate the positions of nucleolar domains. Bar, 10 μm in A–F, 5 μm in G–I.

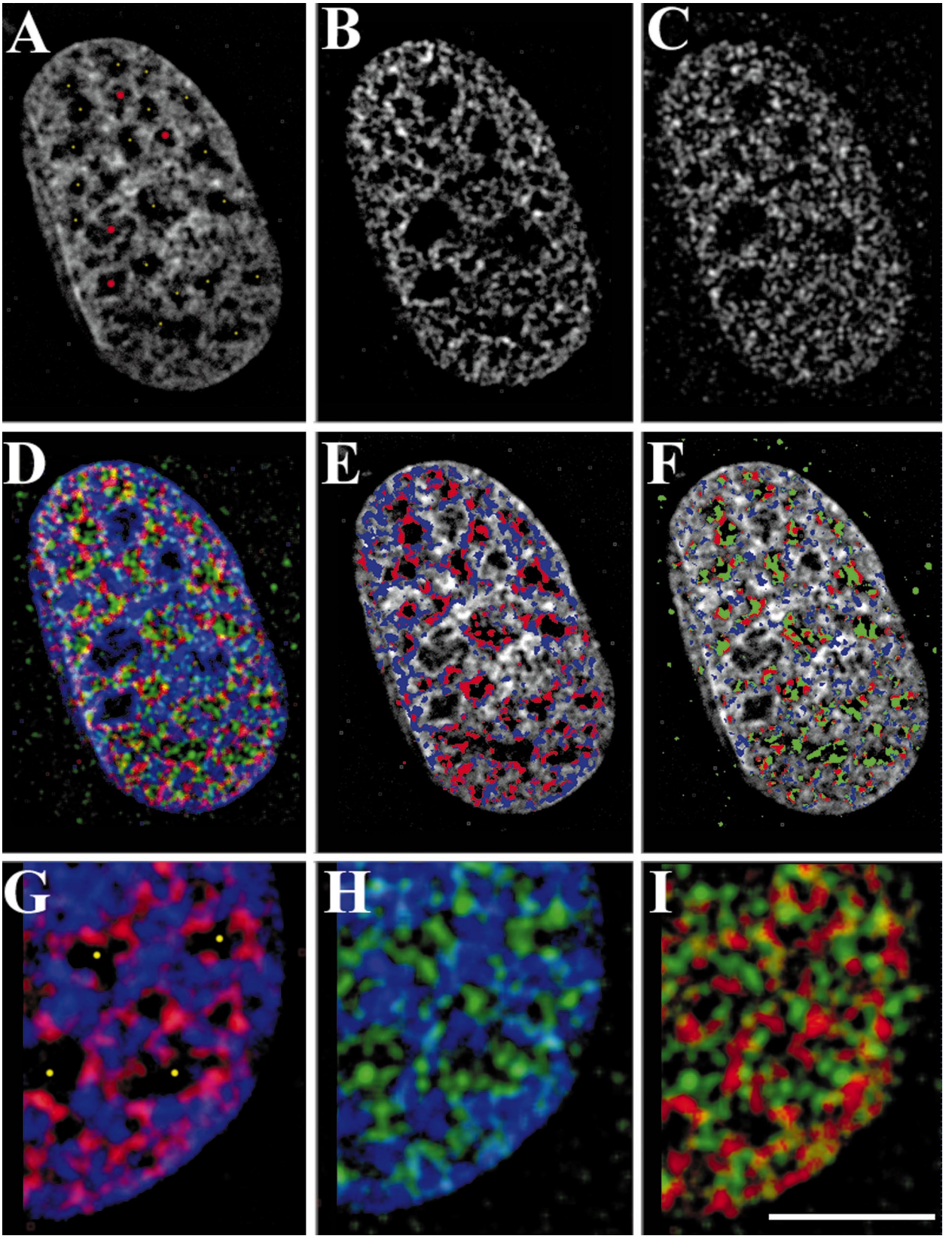

Figure 3.

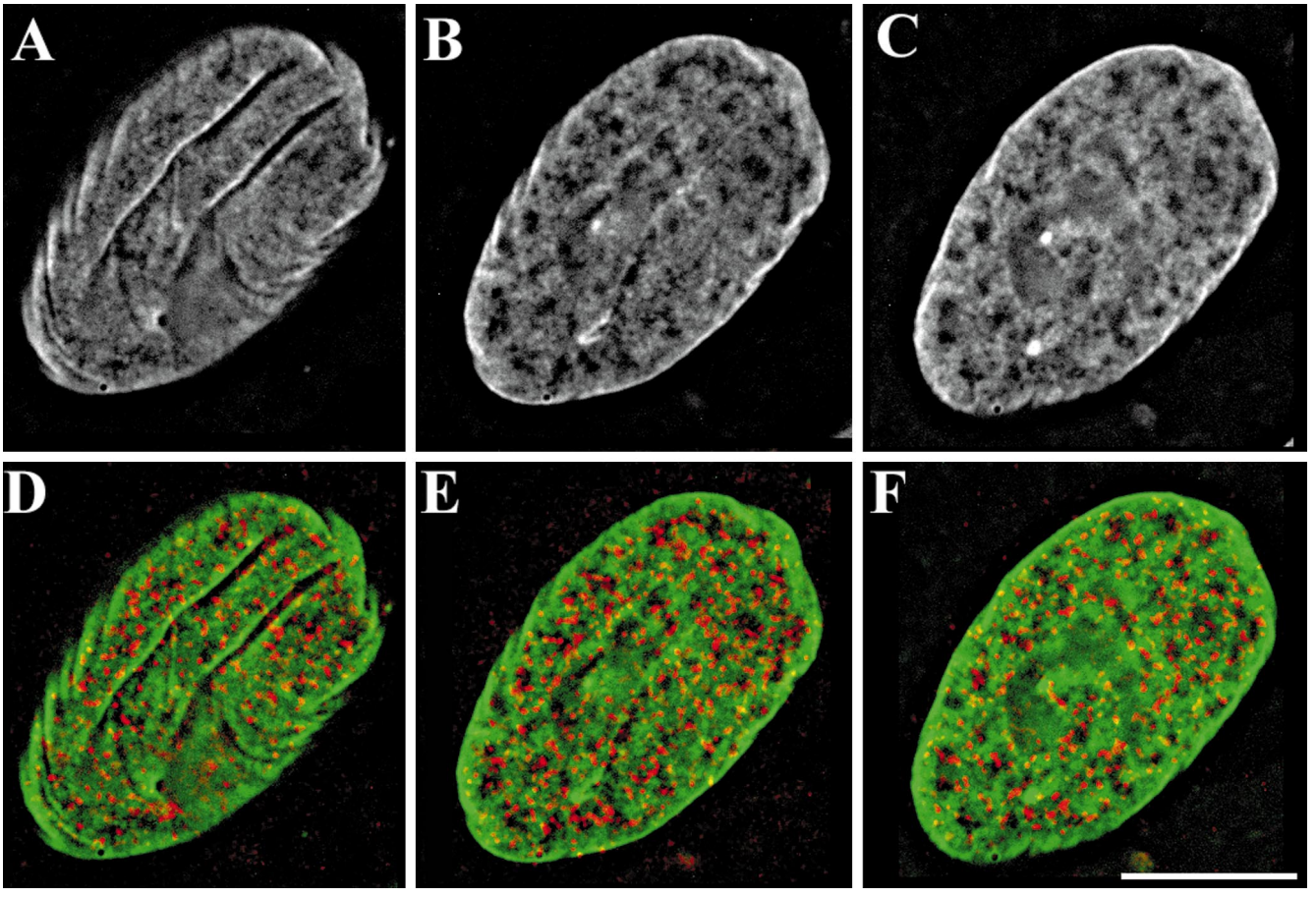

Figure 4. Distribution of HDAC1 in fibroblast cell nuclei. Consecutive digitally deconvolved optical sections of an Indian muntjac fibroblast cell nucleus costained with anti-HDAC-1 and DAPI is shown. Sections of 0.4 μm are shown at 0.8-μm intervals. (A–C) Distribution of DAPI alone. (D–F) Distribution of both DAPI (green) and HDAC-1 (red). Bar, 0.4 μm.

magnification in Figure 3G–I and by thresholding in Figure 3, E and F. In Figure 3E, DAPI is white, DAPI plus acetylated H3 is blue, and acetylated H3 in the absence of detectable DAPI is red. The positions of large extranucleolar chromatin-depleted zones (see Figure 3A, yellow dots), most commonly associated with IGCs, are always enclosed by acetylated chromatin. Large chromatin-depleted domains not encircled by acetylated H3 and which exclude $TAF_{II}250$ are most probably nucleolar regions (Figure 3A, red dots). In contrast to chromatin, foci or elongated foci containing $TAF_{II}250$ infiltrate toward the interior of the IGC-associated chromatin-depleted regions (Figure 3, D, F, H, and I). Figure 3F shows a spatial map of the distribution of $TAF_{II}250$ superimposed on the DAPI image. Regions where $TAF_{II}250$ overlaps with chromatin but where no acetylation is detected (blue) are found throughout the nucleus but are excluded from the immediate nuclear periphery. Areas that contain only $TAF_{II}250$ (green) are predominantly located within IGC-like domains. Of particular interest are the regions where acetylated chromatin and the $TAF_{II}250$ transcription factor–histone acetyltransferase colocalize (red). These regions are enriched at the immediate periphery of the IGC-like domains. These results lead to the tantalizing conclusion that a component of the cell nucleus other than chromatin defines the organization of this common transcription factor and histone acetyltransferase, $TAF_{II}250$. Because much of this nucleoplasmic space is occupied by IGCs, subregions of the IGCs could conceivably be involved in organizing factors such as $TAF_{II}250$. Similar results were obtained with antibodies specific to the CBP histone acetyltransferase (our unpublished results).

Localization of HDAC1

Because the elevated levels of histone acetylation associated with transcriptionally active chromatin have very high turnover rates, it is apparent that highly

acetylated regions of chromatin must recruit HDACs as well as histone acetyltransferases (reviewed in Davie and Hendzel, 1994; Davie, 1996). We used an antibody specific to HDAC1 to determine whether this HDAC is similarly organized in the cell nucleus. Figure 4 shows three 0.4-μm digital optical sections, at 0.8-μm intervals, from a cell costained with anti-HDAC1 (Figure 4D–F, red) and DAPI (Figure 4, A–C, green in D–F). Like highly acetylated chromatin and $TAF_{II}250$, this HDAC is depleted near the periphery of the nucleus. HDAC1 localizes to the periphery of condensed regions of chromatin, and it enriches in chromatin-depleted zones containing IGCs (our unpublished results). Thus, HDAC-1, acetylated chromatin, and $TAF_{II}250$ organizations reflect a spatial association with IGCs and an exclusion from heterochromatic territories of the fibroblast cell nucleus.

The Spatial Relationship between Transcription and Histone Acetylation

To determine directly the relationship between transcriptional activity and histone acetylation, living cells were labeled by the inclusion of bromouridine in the growth medium. Similar methods have recently been used by others (Jackson *et al.*, 1998; Dean Jackson, personal communication). The use of this procedure allows us to label transcription sites without permeabilizing the cell nucleus. This alleviates buffer-mediated changes in chromatin organization, which occur with the bromo-UTP method (our unpublished observations). Figure 5 shows a normal diploid human skin fibroblast that has been incubated for 1 h in the presence of 5 mM bromouridine. Figure 5, top left panel, shows a 0.4-μm digital optical section collected in the DAPI channel. The red dots indicate the positions of nucleoli. The yellow dots indicate the positions of non-nucleolar chromatin-depleted domains characteristic of the positions of IGCs. Figure 5, top right panel, shows the distribution of highly acetylated histone H3 (red) and DAPI (blue). The acetylated chromatin defines the boundaries of the chromatin-depleted zones (Figure 5, top left panel, yellow dots). Similarly, these chromatin-depleted zones contain most of the sites that incorporate bromouridine (Figure 5, bottom left panel, green). In Figure 5, bottom right panel, the relative distributions of condensed chromatin (DAPI, blue), highly acetylated histone H3 (red), and sites of bromouridine incorporation (green) are presented in a composite image. It can be seen that the highly acetylated chromatin that is enriched at the periphery of IGC-like chromatin-depleted zones represents both transcriptionally active (yellow and white) and transcriptionally competent but inactive sequences (red and pink).

Ultrastructure of IGCs and the Surrounding Nucleoplasm

IGCs are recognizable in conventionally prepared TEM sections on the basis of the clustering of a relatively homogeneous population of dense particles. Our immunofluorescent studies on transcriptionally active, competent chromatin organization indicate that the IGC may play both physical and functional roles in interphase chromatin organization. A structural role for IGCs in the organization of interphase chromatin has previously been postulated based on TEM observations (Thiry, 1995). Figure 6 shows a relatively large IGC and its surrounding nucleoplasm. In this image, collected at 155 eV energy loss, phosphorus-containing structures, such as condensed chromatin, show the greatest contrast. Consequently, the IGC appears as a collection of phosphorus-rich particles ~20 nm in diameter. Phosphorus-depleted material, such as protein-rich structures (e.g., PML body), is low in contrast. For example, in Figure 6, the structure enclosed by the box scatters electrons because of its mass but contains little, if any, phosphorus. Structures of similar signal intensity are present throughout the IGC and the surrounding nucleoplasm. Based on their low phosphorus content (our unpublished results), these regions are predominantly protein. Most of the chromatin within the Indian muntjac nucleus is found in small "condensed" domains of chromatin scattered throughout the nucleoplasm. There are, however, some regions of chromatin that appear relatively decondensed (arrows). Chromatin is not observed in the interior of the IGC. Consistent with our immunofluorescent results, many individual regions of chromatin (Figure 6, left panel, white dots) potentially interact with the IGC. However, unlike thick optical sections, which give the impression that chromatin forms a physical barrier limiting the dimensions of the SC-35 domain, ultrathin TEM sections indicate that chromatin does not form a physical boundary to the distribution of interchromatin granules. Thus, the organization of bulk and acetylated chromatin described in Figures 1–5 cannot reflect organization introduced solely by the presence of physical barriers of condensed chromatin as proposed by others (Kramer *et al.*, 1994).

IGCs Are Rich in RNA

We have demonstrated the enrichment of transcriptionally active, competent chromatin at the periphery of IGCs. Consequently, the nature of the interchromatin granule particle would appear to be central to understanding the functional nature of this association. The high contrast generated by interchromatin granules in images collected at 155 eV energy loss indicates the presence of significant quantities of RNA within these particles. However, to be certain that this is not merely a reflection of mass density, it is essential to always gen-

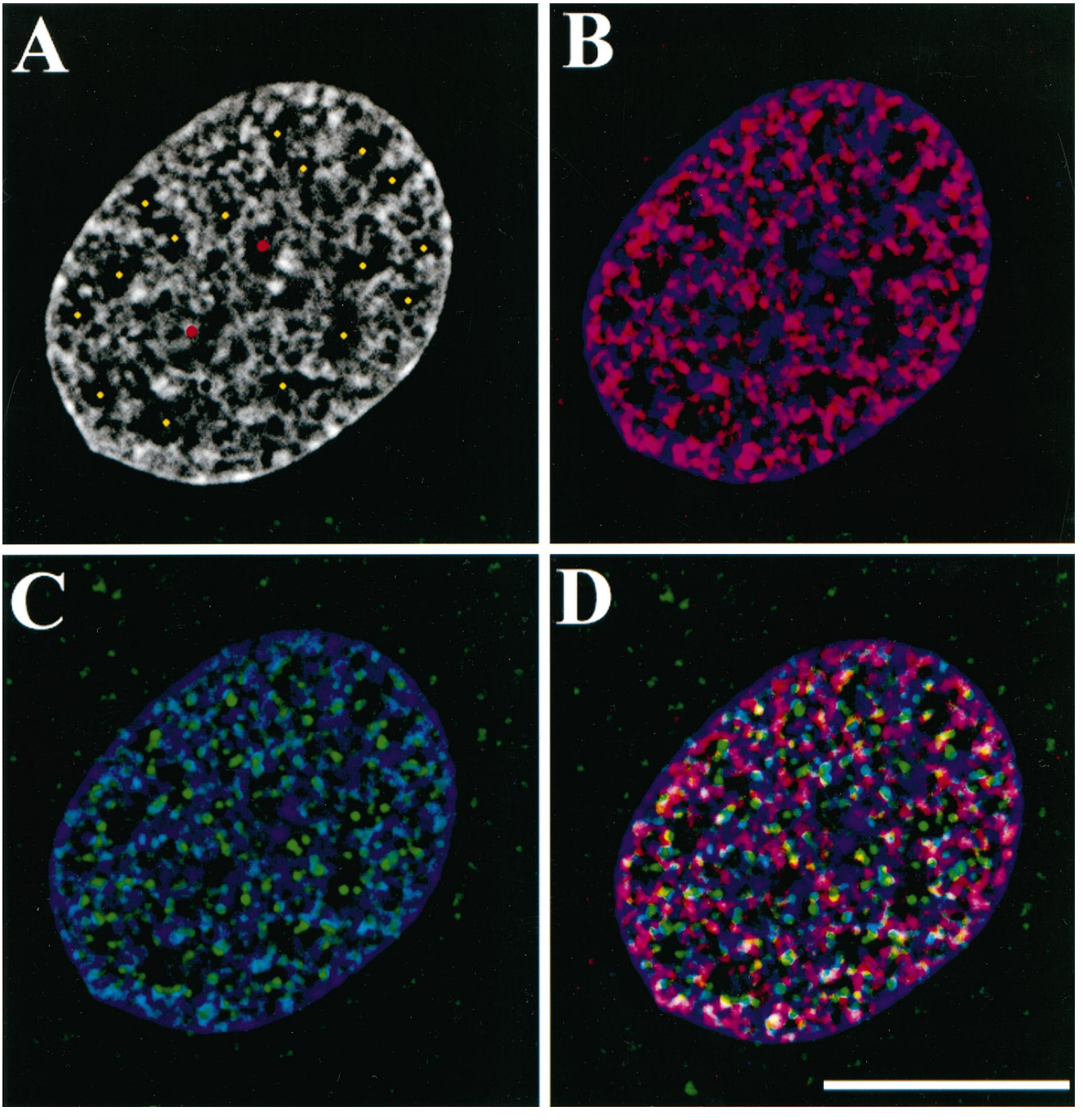

Figure 5. The relationship between highly acetylated chromatin and transcription. Normal human skin fibroblasts were incubated in the presence of 5 mM bromouridine for 1 h, fixed, and then stained with DAPI (top left panel, blue in remaining three panels), anti-highly acetylated histone H3 (red in right panels), and anti-bromouridine (green in bottom panels). The yellow dots indicate the positions of chromatin-depleted IGC-like domains. The red dots indicate the positions of nucleolar domains. Bar, 10 μm.

erate spatial maps of phosphorus distribution using mass-sensitive reference images. These additional images were used in the interpretation of Figure 6.

To better understand the nature of IGCs, we characterized the organization of phosphorus within these domains in cell lines from three species: Indian muntjac, mouse, and human. Indistinguishable results were obtained from each species. Figure 7 shows a particularly well-contrasted image from a mouse 10T½ cell nucleus. In comparing the 120-eV (mass reference image) and

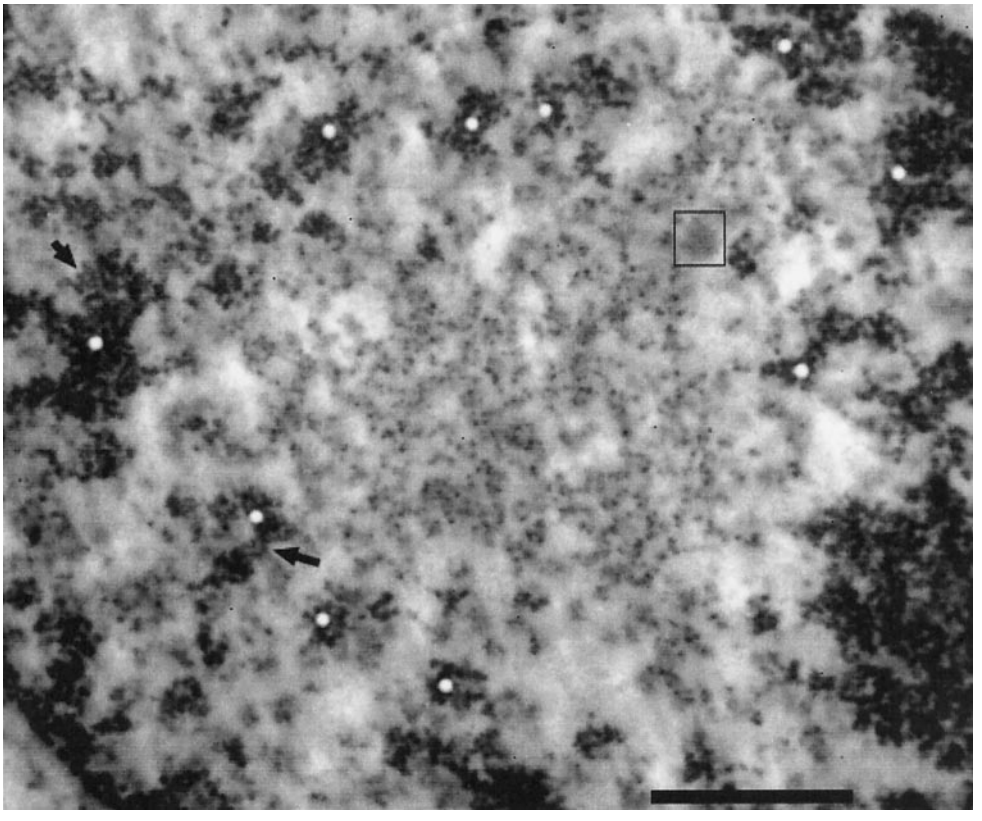

Figure 6. The ultrastructure of IGCs and the surrounding nucleoplasm. Indian muntjac cell nuclei were imaged using ESI at 155 eV energy loss. The white dots indicate small "condensed" regions of chromatin potentially associated with the IGC. The image is displayed as dark on a light background. Bar, 1 μm.

155-eV (phosphorus-enriched) energy loss images, it is apparent that both large (Figure 7, large arrows) and small (Figure 7, small arrows) granular particles show enhanced contrast in the 155-eV image. The size heterogeneity observed in IGCs is not observed in the ribosome population from this section (our unpublished results). Moreover, there are relatively few small particles in the ribosomal regions of the cell (our unpublished results), as expected from the statistical distribution of particles generated by sectioning. Structures, comprising mainly protein, are observed between granules that do not significantly increase in contrast in the 155-eV image. The

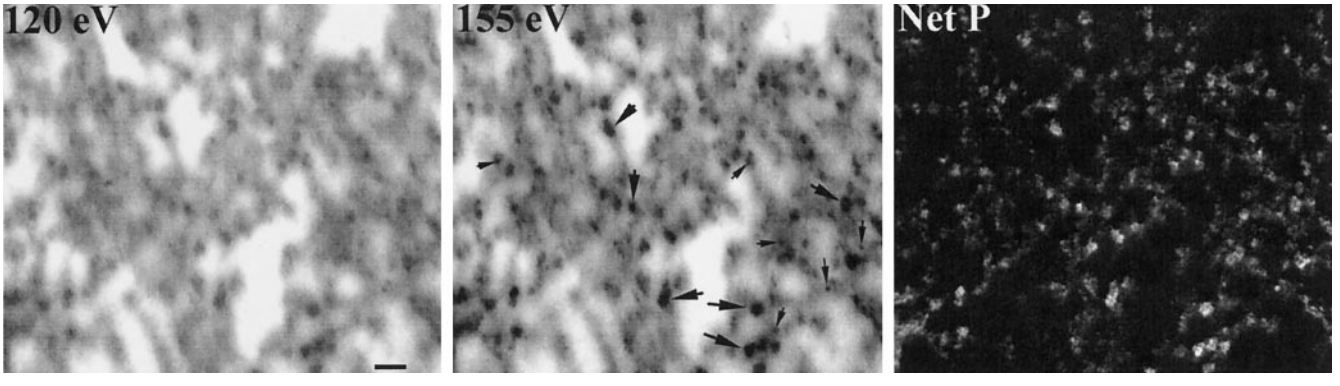

Figure 7. ESI mapping of RNA within the IGC. A mouse 10T½ fibroblast cell nucleus was imaged at 120 eV, and 155-eV energy loss images were collected and used to obtain a net phosphorus image (Net P). Signal in the net phosphorus image is shown as white on black, whereas the 120- and 155-eV images are shown as black on white. The large arrows indicate the positions of interchromatin granule-sized particles within the IGC. The small arrows indicate the position of considerably smaller particles within the IGC that contain significant quantities of phosphorus. Bar, 50 nm.

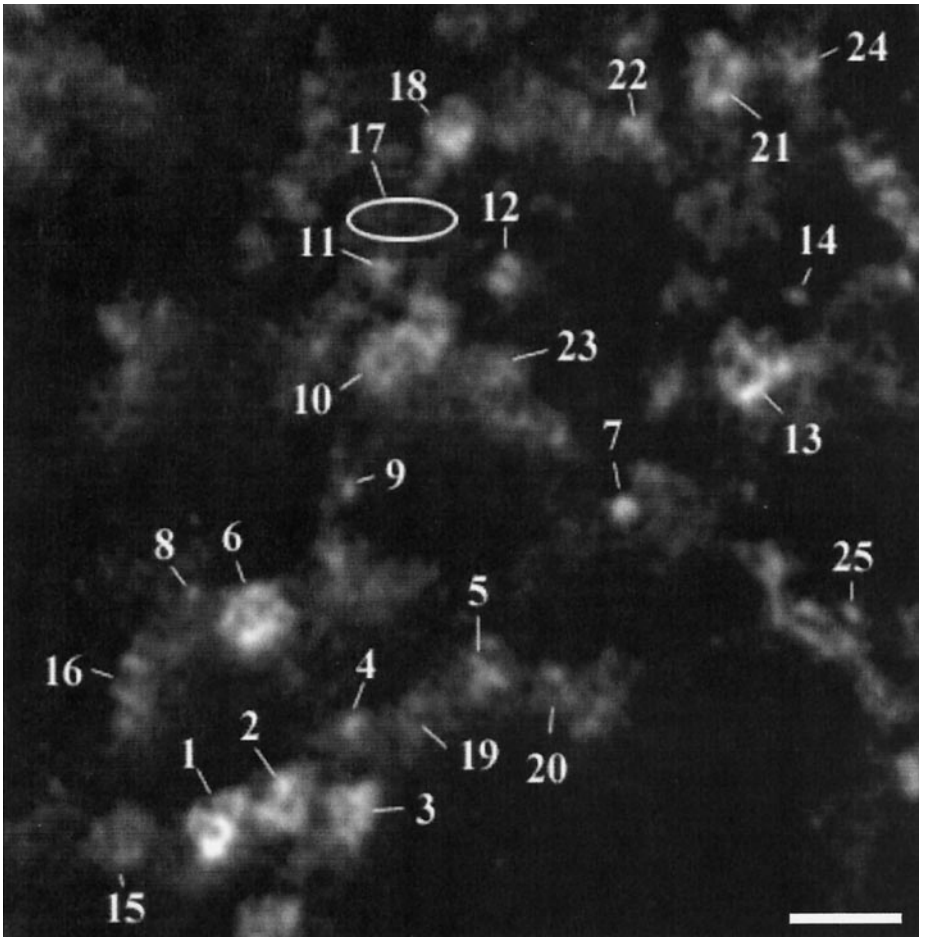

Figure 8. Organization and quantitation of phosphorus within RNPs of the IGC. A subregion of Figure 7 was examined at higher resolutions, and the phosphorus values of individual particles and regions were determined (see Table 1). All regions, with the exception of region 17, are thought to be RNPs. Bar, 50 nm.

net phosphorus map shows a heterogeneous but substantial phosphorus signal arising from both small and large particles.

The phosphorus organization was analyzed in greater detail for a subregion of Figure 7, represented separately in Figure 8. Each large particle, which we define as an interchromatin granule, comprises a highly folded RNP fibril. Each granule appears unique in the manner in which the RNP fibril is folded. However, some similarities are apparent in the subgranular structure of granules 1 and 2 as well as granules 5 and 6. In addition, the density of the RNA within each granule (total phosphorus signal/particle area) varies considerably. A quantitative analysis of these regions is shown in Table 1. The phosphorus signal density generated by the nucleoprotein structures (all regions except 17) are well resolved from the phosphorus signal generated in regions thought to comprised protein only (region 17). The difference between the particle containing the most RNA (particle 10) and the particle containing the least RNA (particle 8) is >40-fold.

Quantitation of RNA within Interchromatin Granules

The biochemical nature of interchromatin granules, which would appear to be central to the function of IGCs, has not been determined. Interchromatin granules are particles that could conceivably correspond to spliceosomes. If IGCs are intranuclear sites of spliceosome storage and/or assembly, as suggested (Huang and Spector, 1996) and indicated by recent imaging studies of living cells (Misteli *et al*., 1997), an abundant nucleoprotein particle consistent with spliceosome composition and size may exist within these sites. The interchromatin granules, although smaller than the reported size of the in vitro mammalian spliceosome (Reed *et al*., 1988), represent potential candidate spliceosomes within IGCs. Phosphorus analysis of particles was undertaken as a means to characterize interchromatin granules. Generally, phosphorus estimates of particles with similar mass densities should be considered accurate within ~20% when photographic film is used to capture the original data. A large num-

Table 1. Quantitation of phosphorous in individual IGs

Particle	Area	Phosphorus density (counts/pixel)	Total phosphorus (AU)
1	125	871.2	108,875
2	104	965.7	81,120
3	99	748.0	74,052
4	16	641	10,256
5	57	556	31,692
6	153	791	121,023
7	21	769	16,149
8	7	510	3,570
9	12	523	6,276
10	260	581	151,060
11	23	589	13,547
12	48	555	26,640
13	175	719	125,825
14	8	682	4,368
15	107	376	40,232
16	88	431	37,928
17	242	165	39,960
18	91	672	61,152
19	45	357	16,065
20	69	529	27,117
21	147	628	92,316
22	27	632	17,364
23	59	488	28,792
24	59	555	32,745
25	12	565	6,780

The regions identified in Figure 8 were quantified for total area, phosphorus counts per area (phosphorus density), and total phosphorus counts. Phosphorus values are expressed as counts detected by the CCD.

ber of interchromatin granules were subjected to quantitative phosphorus analysis to better characterize this population of nuclear RNPs. To eliminate heterogeneity within the population attributable to sampling error, particles were first selected that were roughly spherical, >10 nm in diameter, and were within clusters of similar particles. Data were only collected for particles that appeared as physically isolated individual granules. Subsequently, the population was size resolved, and particles found between the median size ± 0.5 SD units were selected for further analysis. Because ribosomes show less size heterogeneity, ribosomes were not size resolved. The size-resolved interchromatin granules contained 7500 ± 2400 (n = 223) atoms of phosphorus. In comparison, the total ribosome population had a mean phosphorus content of 6600 ± 1100 (n = 112) atoms of phosphorus. These results indicate that interchromatin granules of similar size can contain different amounts of nucleic acid. A histogram plot of the phosphorus contents of total IGs, size-resolved IGs, and the ribosomes is shown in Figure 9. Importantly, the phosphorus content of these particles is considerably greater than that of individual spliceosomes. Rather, the phosphorus content of these particles is most consistent with that of hnRNA.

DISCUSSION

Organization of Highly Acetylated Chromatin

In principle, if chromatin is organized according to function within the cell nucleus, this should be reflected in the organization of highly acetylated chromatin and its associated histone acetyltransferases and deacetylases. Our results demonstrate that highly acetylated chromatin exists in discrete foci within the cell nucleus. This is surprising in light of in vitro experiments using model chromatin templates (Garcia-Ramirez *et al.*, 1995; Schwarz *et al.*, 1996) from which highly acetylated chromatin has long been assumed to exist as isolated and relatively extended polynucleosomal fibers (reviewed in

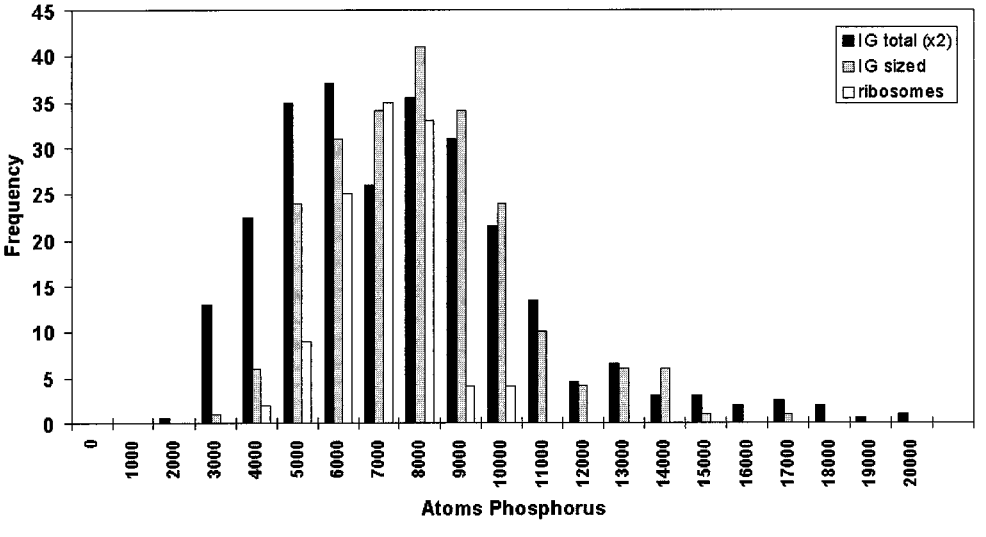

Figure 9. Quantitation of phosphorus within interchromatin granules. A frequency histogram is shown of the measured phosphorus contents of the Indian muntjac interchromatin granule population. Individual granules from interphase cells were quantitated using ribosomes as an internal phosphorus standard. The total interchromatin granule population (the actual frequency is two times the value represented on the y-axis for the total interchromatin granule population), a subset representing the median area ± 0.5 SD, and the ribosome standard are plotted.

Davie, 1996, 1998; also see Armstrong and Emerson, 1998). However, recent investigations into in situ chromatin structure indicate that chromosomes maintain discrete territories (reviewed in Lamond and Earnshaw, 1998) derived from the folding of higher-order "chromonema" fibers (Belmont and Bruce, 1994). Interestingly, regions of chromatin maximally decondensed are prominent on the periphery of the IGC (Belmont and Bruce, 1994). The focal organization that we observe for highly acetylated chromatin may reflect the organization of highly acetylated chromatin into more compact fibers than previously envisioned from biochemical analysis. Our TEM imaging of fibroblast cell nuclei further supports the hypothesis that fibroblasts do not contain substantial amounts of isolated 30- or 10-nm chromatin. Preliminary evidence indicates that the highly acetylated chromatin, identified by indirect immunofluorescence, corresponds to chromatin fibers folded beyond 30 nm (Hendzel *et al*., 1998).

The Spatial Relationship between IGCs and Transcriptionally Active Chromatin

There are many studies that implicate the interface between IGCs and the surrounding nucleoplasm as sites of intense RNA synthesis (reviewed in Clemson and Lawrence, 1996). Furthermore, several endogenous genes whose transcripts are relatively abundant have been shown to be nonrandomly associated with the periphery of IGCs (reviewed in Clemson and Lawrence, 1996). Misteli *et al*. (1997) recently proposed that IGCs function to supply splicing factors to sites of transcription for cotranscriptional processing. Using antibodies specific for the highly acetylated species of histone H3 that are found throughout transcriptionally active and competent regions of interphase chromatin, we demonstrate that the enrichment of transcriptionally active, competent chromatin at the periphery of the IGCs is a general, but not obligatory, feature of euchromatin within fibroblast nuclei. This association reflects an arrangement of several noncontiguous regions of one or more interphase chromosomes on the surface of each IGC. Because only a subset of this chromatin is associated with sites of newly synthesized RNA, this relationship is not solely dependent on transcriptional activity. Thus, although clearly not all transcription occurs at the periphery of IGCs, multiple transcriptionally active regions are located near the periphery of IGCs. This is also reflected in the distribution of highly acetylated chromatin. Earlier TEM autoradiography of thin sections further supports a general enrichment of transcription near IGCs (Fakan and Nobis, 1978; Spector, 1990). We conclude that the phenomenon of the spatial association of active genes with the periphery of IGCs involves the interaction of multiple gene loci with single IGCs.

Recently, based solely on immunofluorescent observations, some have proposed that chromatin remains compacted within chromosomal territories and forms physical barriers that direct the organization of nonchromatin domains such as nuclear speckles (Zirbel *et al*., 1993; Kramer *et al*., 1994). These so-called channeled diffusion models, which could explain our immunofluorescent observations, are not supported by TEM visualization in which chromatin is seen to occupy a small volume of the cell nucleus (see Figure 6). This relative openness of the cell nucleus is apparent when serial optical sections are viewed as three-dimensional projections (our unpublished observations). Based on TEM observations, we propose that the spatial relationship between transcriptionally active chromatin and IGCs is mediated by an active and dynamic process rather than a passive, exclusion-mediated process. Consistent with this interpretation, several recent experiments have implicated active processes in the large-scale chromatin organization of interphase chromatin (reviewed in Lamond and Earnshaw, 1998).

Organization of Histone Acetyltransferases and HDACs

The highly acetylated histones associated with transcriptionally active and competent sequences have characteristically short half-lives in situ (reviewed in Davie and Hendzel, 1994). Biochemical fractionation experiments indicate that histone acetyltransferases and HDACs are components of the nuclear matrix (reviewed in Davie, 1996). This may reflect the sequestration of these enzymes into the nuclear foci that we observe when cells are stained with antibodies specific to individual histone acetyltransferases or deacetylases. Such foci are common for factors involved in RNA polymerase II-mediated gene regulation (Grande *et al*., 1997; Hendzel and Bazett-Jones, unpublished observations) and, at least in some instances, are correlated with in vitro nuclear matrix association (van Steensel *et al*., 1995). Importantly, we demonstrate in this study that the enrichment of foci containing HDAC1 and $TAF_{II}250$ in regions near IGCs correlates well with the in situ distribution of total nuclear histone acetyltransferase and deacetylase activities. In the absence of HDAC inhibitors, foci of highly acetylated chromatin are enriched on the periphery of IGCs. In the presence of HDAC inhibitors, the chromatin at the periphery of IGCs is preferentially hyperacetylated. Thus, both bulk nuclear histone acetyltransferase and HDAC activities enrich in specific regions of the cell nucleus. In the case of $TAF_{II}250$, this localization does not appear to be dictated by the organization of its chromatin substrate. Rather, this protein enriches in a novel subdomain of the nucleus located in the intervening space between the IGC and

surrounding euchromatin. An intriguing possibility is that transcription regulatory factors that act specifically on regions of chromatin, such as histone acetyltransferases, enrich near the surface of IGCs and provide gene specificity to the interactions between the IGC and host chromatin.

IGCs, Splicing Factors, and Spliceosomes

The high enrichment of small nuclear RNAs (snRNAs) and other splicing factors within IGCs indicates that at least some interchromatin granules may be preassembled spliceosomes. The budding of splicing factor-enriched complexes from IGCs and the vectorial transport of these complexes to sites of active transcription implicates IGCs as reservoirs of splicing factors that are targeted to surrounding loci (Misteli *et al*., 1997). A preassembled spliceosome containing single copies of the snRNAs is expected to contain 718 atoms of phosphorus contributed by RNA (Sharp, 1988). Quantitative ESI enabled us to directly evaluate the possibility that interchromatin granules correspond to preassembled but inactive spliceosomes. On average, interchromatin granules contained ~10 times the amount of RNA expected in a spliceosome containing single copies of the snRNAs. Despite this inconsistency, the presence of splicing factors in IGCs is well documented. Some of this mass may be represented in the putative hnRNA-containing particles. However, evidence for recruitment of splicing factors from IGCs indicates that some splicing factors must exist outside of the hnRNA-containing particles. Possibly, snRNAs are present in multiple copies within individual granules. We think that this is unlikely. For example, ~30 copies of the U4/U6 snRNP complex would be required to reconstitute the average of 7700 nucleotides of RNA within an interchromatin granule. With an approximate mass of 250 kDa per snRNP complex (Alberts *et al.*, 1994), the predicted mass of such a particle would be 1.8 times that of the ribosome. Mass-sensitive 120-eV energy loss images are not consistent with this prediction (our unpublished observations). Instead, we suspect that the snRNAs are present as subspliceosomal complexes within IGCs. When images were collected with improved sensitivity using a 14-bit CCD, we could observe, dispersed within the intergranular protein, smaller RNP complexes. Although accurate quantitation was not possible, we estimate that these particles contain as few as 200–300 atoms of phosphorus, which is close to the phosphorus values expected for the RNA components of the U1, U2, U4/U6, and U5 complexes. Thus, we suspect that the snRNAs are found within the small RNPs located outside of the interchromatin granules but within the IGC (see Figures 7 and 8).

What Are Interchromatin Granules?

There is evidence that both specific endogenous pre-mRNAs (reviewed in Clemson and Lawrence, 1996) and, upon infection, viral pre-mRNAs (reviewed in Bridge and Pettersson, 1996; Puvion and Puvion-Dutilleul, 1996) enrich within IGCs. There is further evidence that both rapid-turnover poly(A) RNA (Visa *et al*., 1993) and slow-turnover poly(A) RNA (Huang *et al.*, 1994; Fay *et al*., 1997) accumulate within interchromatin granules. Although it is clear that IGCs label only weakly in experiments designed to detect RNA metabolically (reviewed in Puvion and Puvion-Dutilleul, 1996), it is also clear that there is a significant amount of RNA present within IGCs (Thiry, 1993). Despite some experimental evidence that highly phosphorylated proteins are, in part, responsible for the contrasting of interchromatin granules using the EDTA-regressive staining method of Bernhard (1969) (Wassef, 1979), the density of phosphate incorporated into even the most highly phosphorylated proteins in situ would not significantly influence the quantitation of phosphorus in a nucleoprotein. For example, if an extremely high estimate of 25 phosphorylations per 100 KDa is allowed and a protein component of ~2 MDa (the approximate protein content of the ribosome), then a maximum of 500 phosphorus atoms can be contributed by protein. Clearly this is an overestimate. Thus, our quantitative estimates of the phosphorus content of interchromatin granules provide direct evidence for the presence of substantial quantities of RNA within these particles. We estimate that the interchromatin granules contain, on average, 7700 nucleotides of RNA. Of the two known RNA components of IGCs, the poly(A) hnRNA component is most likely to provide all or most of the RNA component of the interchromatin granule. The variability of the RNA content within the population of interchromatin granules is further consistent with the representation of a variety of sequences within the IGC, rather than a more homogenous composition characteristic of a defined RNA content, such as is observed with the ribosome population.

Although we interpret the phosphorus content of interchromatin granules to reflect the presence of hnRNA, our results are not consistent with the expected size of individual fully processed nuclear pre-mRNAs. Biochemical experiments using pulse labeling of nuclear RNA demonstrated that newly synthesized RNA is, on average, ~7000 nucleotides in length. The length of transcript changes during a brief chase to an average of ~1500 nucleotides in average length (Alberts *et al*., 1994). Thus, if our results reflect the presence of single RNA copies within individual particles, they indicate that the species of RNA that tend to accumulate within IGCs reflect either unprocessed transcripts or are biased toward RNAs of longer

lengths. However, it is also possible that multiple copies of fully processed transcripts are present within single interchromatin granules. Some experimental evidence supports the existence of multiple copies of RNAs within single nuclear mRNA-containing particles (D. Jackson, personal communication). Consequently, our results are also consistent with the presence of approximately five copies of fully processed RNAs per particle.

Although the phosphorus content of interchromatin granules is likely to be generated by hnRNA, the nature of the hnRNA within these particles is less certain. In particular, it should be noted that, with the possible exception of the poly(rG) binding hnRNPs F and H (Matunis *et al.*, 1994), hnRNPs, unlike poly(A) RNA and splicing factors, do not appear to enrich within IGCs (Fakan *et al.*, 1984). These results, however, are not straightforward to interpret, because epitope accessibility could change if, for example, perichromatin fibrils were compared with a perichromatin fibril-based granule. Our high-resolution phosphorus mapping of interchromatin granules indicate the presence of highly folded RNA-rich fibrils. Consequently, epitope accessibility may influence the detection of hnRNP antigens within IGCs. Alternatively, the interchromatin granules may represent a novel class of RNA that has a long half-life and is polyadenylated. Evidence to support this hypothesis is presented and reviewed by Huang *et al.* (1994). In this instance, the absence of associated hnRNP antigens may reflect a novel protein composition to these RNP granules. These two hypotheses need not be mutually exclusive.

ACKNOWLEDGMENTS

We thank Manfred Herfort and Maryse Fillion for excellent technical assistance. We thank Dr. C.D. Allis for the gift of acetylated histone H3 and acetylated H4 antibodies and Dr. Dean Jackson for communicating results before publication. This project was supported by operating grants from the Medical Research Council of Canada and the Cancer Research Society to D.P.B.-J.

REFERENCES

Abholhassani-Dadras, S., Vazquez-Nin, G.H., Echeverria, O.M., and Fakan, S. (1996). Image-EELS for in situ estimation of the phosphorus content of RNP granules. J. Micros. *183*, 215–222.

Alberts, B., Bray, D., Lewis, J., Raff, M., Roberts, K., and Watson, J.D. (1994). Molecular Biology of the Cell, 3rd ed., New York: Garland Publishing, 233.

Armstrong, J.A., and Emerson, B.M. (1998). Transcription of chromatin: these are complex times. Curr. Opin. Genet. Dev. *8*, 165–172.

Bazett-Jones, D.P. (1992). Empirical basis for phosphorus mapping and structure determination of DNA:protein complexes by electron spectroscopic imaging. Microbeam Analysis *2*, 69–79.

Belmont, A.S., and Bruce, K. (1994). Visualization of G1 chromosomes—a folded, twisted, supercoiled chromonema model of interphase chromatid structure. J. Cell Biol. *127*, 287–302.

Bernhard, W. (1969). A new staining procedure for electron microscopical cytology. J. Ultrastruct. Res. *27*, 250–265.

Boffa, L.C., Walker, J., Chen, T.A., Sterner, R., Mariani, M.R., and Allfrey, V.G. (1990). Factors affecting nucleosome structure in transcriptionally active chromatin. Histone acetylation, nascent RNA and inhibitors and RNA synthesis. Eur. J. Biochem. *194*, 811–823.

Boggs, B.A., Connors, B., Sobel, R.E., Chinault, A.C., and Allis, C.D. (1996). Reduced levels of histone H3 acetylation on the inactive X chromosome in human females. Chromosoma *105*, 303–309.

Breneman, J.W., Yau, P.M., Swiger, R.R., Teplitz, R., Smith, H.A., Tucker, J.D., and Bradbury, E.M. (1996). Acivity banding of human chromosomes as shown by histone acetylation. Chromosoma *105*, 41–49.

Bridge, E., Riedel, K.-U., Johansson, B.-M., and Pettersson, U. (1996). Spliced exons of adenovirus late RNAs colocalize with snRNP in a specific nuclear domain. J. Cell Biol. *135*, 303–314.

Bridge, E., and Pettersson, U. (1996). Nuclear organization of adenovirus RNA biogenesis. Exp. Cell Res. *229*, 233–239.

Carter, K.C., Bowman, D., Carrington, W., Fogarty, K., McNeil, J.A., Fay, F.S., and Lawrence, J.B. (1993). A three-dimensional view of precursor messenger RNA metabolism within the mammalian nucleus. Science *259*, 1330–1334.

Carter, K.C., Taneja, K.L., and Lawrence, J.B. (1991). Discrete nuclear domains of poly(A) RNA and their relationship to the functional organization of the nucleus. J. Cell Biol. *115*, 1191–1202.

Clemson, C.M., and Lawrence, J.B. (1996). Multifunctional compartments in the nucleus: insights from DNA and RNA localization. J. Cell. Biochem. *62*, 81–190.

Covault, J., and Chalkley, R. (1980). The identification of distinct populations of acetylated histone. J. Biol. Chem. *255*, 9110–9116.

Davie, J.R. (1996). Histone modifications, chromatin structure, and the nuclear matrix. J. Cell. Biochem. *62*, 454–466.

Davie, J.R. (1998). Covalent modification of histones: expression from chromatin templates. Curr. Opin. Genet. Dev. *8*, 173–178.

Davie, J.R., and Hendzel, M.J. (1994). The multiple functions of dynamic histone acetylation. J. Cell. Biochem. *55*, 98–105.

Fakan, S (1994). Perichromatin fibrils are in situ forms of nascent transcripts. Trends Cell Biol. *4*, 86–90.

Fakan, S., and Bernhard, W. (1973). Nuclear labelling after prolonged ^{3}H-uridine incorpporation as visualized by high resolution autoradiography. Exp. Cell Res. *79*, 431–444.

Fakan, S., Leser, G., and Martin, T.E. (1984). Ultrastructural distribution of nuclear ribonucleoproteins as visualized by immunocytochemistry on thin sections. J. Cell Biol. *98*, 358–363.

Fakan, S., and Nobis, P. (1978). Ultrastructural localization of transcription sites and of RNA distribution during the cell cycle of synchronized CHO cells. Exp. Cell Res. *113*, 327–337.

Fakan, S., and Puvion, E. (1980). The ultrastructural visualization of nucleolar and extranucleolar RNA synthesis and distribution. Int. Rev. Cytol. *65*, 255–299.

Fay, F.S., Taneja, K.L., Shenoy, S., Lifshitz, L., and Singer, R.H. (1997). Quantitative digital analysis of diffuse and concentrated nuclear distributions of nascent transcripts, SC35, and poly(A). Exp. Cell Res. *231*, 23–37.

Ferreira, J., Paolella, G., Ramos, C., and Lamond, A.I. (1997). Spatial organization of large-scale chromatin domains in the nucleus: a magnified view of single chromosome territories. J. Cell Biol. *139*, 1597–1610.

Fu, X.D., and Maniatis, T. (1990). Ractor required for mammalian spliceosome assembly is localized to discrete regions in the nucleus. Nature *343*, 437–441.

Garcia-Ramirez, M., Rocchini, C., and Ausio, J. (1995). Modulation of chromatin folding by histone acetylation. J. Biol. Chem. *270*, 17923–17928.

Grande, M.A., van der Kraan, I., de Jong, L., and van Driel, R. (1997). Nuclear distribution of transcription factors in relation to sites of transcription and RNA polymerase II. J. Cell Sci. *110*, 1781–1791.

Hendzel, M.J., and Bazett-Jones, D.P. (1996). Probing nuclear ultrastructure by electron spectroscopic imaging (ESI). J. Microsc. *182*, 1–14.

Hendzel, M.J., Delcuve, G.P., and Davie, J.R. (1991). Histone deacetylase is a component of the internal nuclear matrix. J. Biol. Chem. *266*, 21936–21942.

Hendzel, M.J., Kruhlak, M.J., and Bazett-Jones, D.P. (1998). Electron spectroscopic imaging and correlative fluorescent microscopy of the cell nucleus. Scanning (*in press*).

Hendzel, M.J., Sun, J.-M., Chen, H.Y., Rattner, J.B., and Davie, J.R. (1994). Histone acetyltransferase is associated with the nuclear matrix. J. Biol. Chem. *269*, 22894–22901.

Huang, S., Deerinck, T.J., Ellisman, M.H., and Spector, D.L. (1994). In vivo analysis of the stability and transport of nuclear poly(A)$^+$ RNA. J. Cell Biol. *126*, 877–899.

Huang, S., and Spector, D.L. (1991). Nascent pre-mRNA transcripts are associated with nuclear regions enriched in splicing factors. Genes Dev. *5*, 2288–2302.

Huang, S., and Spector, D.L. (1996). Dynamic organization of pre-mRNA splicing factors. J. Cell. Biochem. *62*, 191–197.

Ishov, A.M., Stenberg, R.M., and Maul, G.G. (1997). Human cytomegalovirus immediate early interaction with host nuclear structures: definition of an immediate transcript environment. J. Cell Biol. *138*, 5–16.

Jackson, D.A., Iborra, F.I., Manders, E.M.M., and Cook, P.R. (1998). Numbers and organization of RNA polymerases, nascent transcript and transcription units in HeLa nuclei. Mol. Biol. Cell *9*, 1523–1536.

Jeppesen, P. (1997). Histone acetylation: a possible mechanism for the inheritance of cell memory at mitosis. Bioessays *19*, 67–74.

Kramer, J., Zachar, Z., and Bingham, P.M. (1994). Nuclear pre-mRNA metabolism: channels and tracks. Trends Cell Biol. *4*, 35–37.

Lamond, A.I., and Earnshaw, W.C. (1998). Structure and function in the nucleus. Science *280*, 547–553.

Matunis, M.J., Xing, J., and Dreyfuss, G. (1994). The hnRNP F protein: unique primary structure, nucleic acid-binding properties, and subcellular localization. Nucleic Acids Res. *22*, 1059–1067.

Misteli, T., Caceres, J.F., and Spector, D.L. (1997). The dynamics of a pre-mRNA splicing factor in living cells. Nature *387*, 523–527.

Misteli, T., and Spector, D.L. (1997). Protein phosphorylation and the nuclear organization of pre-mRNA splicing. Trends Cell Biol. *7*, 135–138.

Mizzen, C.A., *et al*. (1996). The TAF(II)250 subunit of TFIID has histone acetyltransferase activity. Cell *87*, 1261–1270.

Monneron, A., and Bernhard, W. (1969). Fine structural organization of the interphase nucleus in some mammalian cells. J. Ultrastruct. Res. *27*, 266–288.

Nevins, J.R., and Darnell, J.E., Jr. (1978). Steps in the processing of Ad2 mRNA: poly(A)+ nuclear sequences are conserved and poly(A) addition precedes splicing. Cell *15*, 1477–1493.

Puvion, E., and Puvion-Dutilleul, F. (1996). Ultrastructure of the nucleus in relation to transcription and splicing: roles of perichromatin fibrils and interchromatin granules. Exp. Cell Res. *229*, 217–225.

Raska, I. (1995). Nuclear ultrastructures associated with the RNA synthesis and processing. J. Cell. Biochem. *59*, 11–26.

Rattner, J.B., Hendzel, M.J., Furbee, C.S., Muller, M.T., and Bazett-Jones, D.P. (1996). Topoisomerase II is associated with the mammalian centromere in a cell cycle- and species-specific manner and is required for proper centromere/kinetochore structure. J. Cell Biol. *134*, 1097–1107.

Reed, R., Griffith, J., and Maniatis, T. (1988). Purification and visualization of native spliceosomes. Cell *53*, 949–961.

Robinett, C.C., Straight, A., Li, G., Willhelm, C., Sudlow, G., Murray, A., and Belmont, A.S. (1996). In vivo localization of DNA sequences and visualization of large-scale chromatin organization using lac operator/repressor recognition. J. Cell Biol. *135*, 1685–1700.

Ruppert, S., Wang, E.H., and Tjian, R. (1993). Cloning and expression of human $TAF_{II}250$: a TBP-associated factor implicated in cell-cycle regulation. Nature *362*, 175–179.

Schwarz, P.M., Felthauser, A., Fletcher, T.M., and Hansen, J.C. (1996). Reversible oligonucleosome self-association: dependence on divalent cations and core histone tail domains. Biochemistry *35*, 4009–4015.

Sharp, P.A. (1988). RNA splicing and genes. JAMA *260*, 3035–3041.

Spector, D.L. (1990). Higher order nuclear organization: three-dimensional distribution of small nuclear ribonucleoprotein particles. Proc. Natl. Acad. Sci. USA *87*, 147–151.

Spector, D.L. (1996). Nuclear organization and gene expression. Exp. Cell Res. *229*, 189–197.

Spector, D.L., Fu, X.-D., and Maniatis, T. (1991). Associations between distinct pre-mRNA splicing components and the cell nucleus. EMBO J. *11*, 3467–3481.

Strouboulis, J., and Wolffe, A.P. (1996). Functional compartmentalization of the nucleus. J. Cell Sci. *109*, 1991–2000.

Thiry, M. (1993). Differential location of nucleic acids within interchromatin granule clusters. Eur. J. Cell Biol. *62*, 259–269.

Thiry, M. (1995). Behaviour of interchromatin granules during the cell cycle. Eur. J. Cell Biol. *68*, 14–24.

van Steensel, B., Brink, M., van der Meulen, K., van Binnendijk, E.P., Wansink, D.G., de Jong, L., de Kloet, E.R., and van Driel, R. (1995). Localization of the glucocorticoid receptor in discrete clusters in the cell nucleus. J. Cell Sci. *108*, 3003–3011.

Visa, N., Puvion-Dutilleul, F., Harper, F., Bachellerie, J.-P., and Puvion, E. (1993). Intranuclear distribution of poly(A) RNA determined by electron microscope in situ hybridization. Exp. Cell Res. *208*, 19–34.

Wassef, M. (1979). A cytochemical study of interchromatin granules. J. Ultrastruct. Res. *69*, 121–133.

Xing, Y., Johnson, C.V., Dobner, P.R., and Lawrence, J.B. (1993). Higher-level organization of individual gene transcription and RNA splicing. Science *259*, 1326–1330.

Xing, Y., Johnson, C.V., Moen, P.T., Jr., McNeil, J.A., and Lawrence, J.B. (1995). Nonrandom gene organization: structural arrangements of specific pre-mRNA transcription and splicing with SC-35 domains. J. Cell Biol. *131*, 1635–1647.

Zirbel, R.M., Mathieu, U.R., Kurz, A., Cremer, T., and Lichter, P. (1993). Evidence for a nuclear compartment of transcription and splicing located at chromosome domain boundaries. Chromosome Res. *1*, 93–106.